



Influence of acidity on liquid–liquid phase transitions of mixed secondary organic aerosol (SOA) proxy–inorganic aerosol droplets

Yueling Chen^{1,★}, Xiangyu Pei^{1,★}, Huichao Liu¹, Yikan Meng¹, Zhengning Xu¹, Fei Zhang¹, Chun Xiong¹, Thomas C. Preston^{3,4}, and Zhibin Wang^{1,2}

¹Zhejiang Provincial Key Laboratory of Organic Pollution Process and Control, MOE Key Laboratory of Environment Remediation and Ecological Health, College of Environmental and Resource Sciences, Zhejiang University, Hangzhou 310058, China

²ZJU-Hangzhou Global Scientific and Technological Innovation Center, Zhejiang University, Hangzhou 311215, China

³Department of Atmospheric and Oceanic Sciences, McGill University, 805 Sherbrooke Street West, Montréal, Quebec H3A 0B9, Canada

⁴Department of Chemistry, McGill University, 805 Sherbrooke Street West, Montréal, Quebec H3A 0B9, Canada

★These authors contributed equally to this work.

Correspondence: Zhibin Wang (wangzhibin@zju.edu.cn)

Received: 8 April 2023 – Discussion started: 21 April 2023

Revised: 1 August 2023 – Accepted: 7 August 2023 – Published: 14 September 2023

Abstract. The phase state and morphology of aerosol particles play a critical role in determining their effect on climate. While aerosol acidity has been identified as a key factor affecting multiphase chemistry and phase transitions, the impact of acidity on the phase transition of multicomponent aerosol particles has not been extensively studied in situ. In this work, we employed aerosol optical tweezers (AOT) to probe the impact of acidity on the phase transition behavior of levitated aerosol particles. Our results revealed that higher acidity decreases the separation relative humidity (SRH) of aerosol droplets mixed with ammonium sulfate (AS) and secondary organic aerosol (SOA) proxy, such as 3-methylglutaric acid (3-MGA), 1,2,6-hexanetriol (HEXT) and 2,5-hexanediol (HEXD) across aerosol pH in atmospheric conditions. Phase separation of organic acids was more sensitive to acidity compared to organic alcohols. We found the mixing relative humidity (MRH) was consistently higher than the SRH in several systems. Phase-separating systems, including 3-MGA / AS, HEXT / AS and HEXD / AS, exhibited oxygen-to-carbon ratios (O : C) of 0.67, 0.50 and 0.33, respectively. In contrast, liquid–liquid phase separation (LLPS) did not occur in the high-O : C system of glycerol / AS, which had an O : C ratio of 1.00. Additionally, the morphology of 42 out of the 46 aerosol particles that underwent LLPS was observed to be a core–shell structure. Our findings provide a comprehensive understanding of the pH-dependent LLPS in individual suspended aerosol droplets and pave the way for future research on phase separation of atmospheric aerosol particles.

1 Introduction

Atmospheric aerosol particles can directly and indirectly impact climate by absorbing and scattering light and acting as cloud condensation nuclei (Rosenfeld et al., 2014). Particle morphology is a critical factor influencing the physiochemical properties of aerosols such as their optical properties, chemistry and nucleation processes (Freedman et al., 2009; Corral Arroyo et al., 2022; Cosman et al., 2008; Lam et al., 2021; Petters and Kreidenweis, 2007; Mikhailov et al., 2021). Morphology can be broadly categorized into single-phase homogeneous morphology and phase separation morphology (Bertram et al., 2011; Ciobanu et al., 2009), based on the phase state of the particle. For droplets with a phase separation morphology, the two main equilibrium morphologies are a fully engulfed (core–shell) structure and a partially engulfed structure (Reid et al., 2011). Droplets can undergo phase transition processes, and thus their morphology can change. The composition and mass of inorganic and organic components impact the phase transition characteristics of a particle. With a decrease in particle water content, a transition occurs from a single homogeneous liquid phase to two separated liquid phases, which is known as liquid–liquid phase separation (LLPS; Freedman et al., 2017). The relative humidity (RH) when the LLPS occurs is defined as separation relative humidity (SRH). The reverse process, in which two liquid phases mix into a single homogeneous liquid phase, is referred to as liquid–liquid phase mixing, and the corresponding RH is the mixing RH (MRH; You et al., 2014; Gorkowski et al., 2017).

The phenomenon of LLPS has garnered considerable attention from the atmospheric research community due to its potential role in affecting the physiochemical properties of atmospheric aerosols (Kucinski et al., 2019; Ott et al., 2020; Freedman, 2020). Song et al. (2012), using optical microscopy, studied the relationship between LLPS and the oxygen-to-carbon ratio (O : C) and discovered that LLPS was consistently observed when $O : C < 0.56$, while it was never observed when $O : C > 0.80$. For $O : C$ between 0.56 and 0.80, the occurrence of LLPS was influenced by the types of organic functional groups. Gorkowski et al. (2020) utilized experimental results of previous studies on LLPS and morphology, observing a general trend in morphology from partially engulfed to core–shell and finally homogeneous structure as oxidation increased. More recently, it has been found that submicrometer-sized aerosol particles have a lower SRH compared to micrometer-sized droplets (Kucinski et al., 2021; Ohno et al., 2021). Meanwhile, Stewart et al. (2015) employed aerosol optical tweezers (AOT) to investigate the morphologies of aqueous droplets. They found in the polyethylene glycol (PEG) / ammonium sulfate (AS) system that droplets formed predominately core–shell particles when the AS content was high and were partially engulfed when the PEG content was high.

One factor that could influence the phase transitions of aerosol particles is the aerosol pH. The pH values for misty cloud and fog droplets generally range between 2 and 7, whereas continental and marine aerosol particles exhibit a wider range of pH values, from -1 to 5 and 0 to 8, respectively (Pye et al., 2020; Angle et al., 2021; Weber et al., 2016; Tilgner et al., 2021; Zheng et al., 2020). Meanwhile, aerosol pH is size-dependent, with the fine mode showing lower pH 1–4 units than the coarse mode (Fang et al., 2017; Young et al., 2013; Guo et al., 2017). Losey et al. (2018) studied six organic components and discovered that phase separation may be hindered by the addition of sulfuric acid, while the SRH of the 3-methylglutaric acid / ammonium sulfate system was found to decrease with the addition of sodium hydroxide (Losey et al., 2016), as the deprotonation of the organic component or difference in the salting-out ability of the inorganic component may change the SRH. More recently, Tong et al. (2022) investigated the effect of acidity on phase separation in single suspended microdroplets using AOT. Their results showed that the pH can affect the miscibility of the mixture and that high acidity results in a reduced SRH of 1,2,6-hexanetriol.

Our aim with this work is to gain a comprehensive understanding of the influence of pH on phase transitions in suspended droplets. To that end, we investigated pH-dependent SRH and MRH, as well as morphologies of aqueous droplets using AOT, and also discussed the effect of O : C on phase separation behavior. Compared to substrate-based measurement techniques, AOT can suspend droplets without any substrate contact, providing a more realistic simulation of the behavior of aerosols in the atmosphere (Wang et al., 2021; Cui et al., 2021; Redding et al., 2015; Gong et al., 2018; Rafferty et al., 2023). We measured droplets containing AS and a range of organic compounds with varying O : C. Our findings provide insight into the mechanisms behind pH-dependent phase transitions in levitated droplets and have implications for fields such as climate science. Overall, our study highlights the importance of considering pH as a key factor in the phase transition behavior of micrometer-sized droplets and underscores the need for further research to fully understand the complex interactions between pH and phase transitions in these atmospherically relevant systems.

2 Methods

2.1 Aerosol generation

Four organic components, glycerol (GL), 3-methylglutaric acid (3-MGA), 1,2,6-hexanetriol (HEXT) and 2,5-hexanediol (HEXD), were chosen as they are commonly used secondary organic aerosol (SOA) proxies (Lam et al., 2021; Gorkowski et al., 2020). The O : C ratio of the selected chemicals varied from 1 to 0.33 (Table 1), which is similar to the real atmospheric SOA (Canagaratna et al., 2015; Mahrt et al., 2021). AS was chosen as the inorganic

Table 1. Information on the solutions used to generate aerosol droplets.

Solution ID	Organic component	O : C ratio	pH
GL	glycerol	1.00	5.24 ± 0.01
3-MGA-I	3-methylglutaric acid	0.67	0.48 ± 0.01
3-MGA-II			1.19 ± 0.01
3-MGA-III			2.70 ± 0.01
3-MGA-IV			3.70 ± 0.01
3-MGA-V			5.21 ± 0.02
3-MGA-VI			6.53 ± 0.02
HEXT-I	1,2,6-hexanetriol	0.50	0.92 ± 0.01
HEXT-II			2.02 ± 0.01
HEXT-III			3.14 ± 0.01
HEXT-IV			5.11 ± 0.02
HEXD-I	2,5-hexanediol	0.33	1.39 ± 0.01
HEXD-II			2.03 ± 0.01
HEXD-III			2.71 ± 0.01
HEXD-IV			3.13 ± 0.01
HEXD-V			5.01 ± 0.01

salt component due to its widespread occurrence in the atmospheric environment. All concentrations of organics and AS in the mother solutions were 50 g L⁻¹. The pure organic and inorganic components were dissolved in ultrapure water (Millipore, resistivity of 18.2 MΩ) to create solutions with an organic-to-inorganic mass ratio (OIR) of 1 : 1. The pH of studied systems was adjusted to within the range of 0.48 to 6.53 by using either concentrated sulfuric acid (SA) or sodium hydroxide (NaOH) solution (5.29 mol L⁻¹). Sodium hydroxide, a strong base, allowed for pH adjustment with minimal usage (Losey et al., 2016). However, it is necessary to acknowledge that the addition of NaOH changed the composition of the inorganic part of the solution, potentially affecting the SRH values measured. The pH of each solution was measured using a pH meter (Mettler Toledo, Shanghai, China). The purities and suppliers of the compounds used in this study are summarized in Table S1 in the Supplement.

2.2 Experimental setup

A schematic illustration of the experimental setup is presented in Fig. S1. The aerosol optical tweezer system consists of a custom-made levitation chamber that integrates the optical trapping system, the illumination and imaging system, and the aerosol generation system. A 532 nm (2 W opus 532) laser was used to create an optical trap with a 100× oil immersion objective (Olympus, UPLFLN100XO, numerical aperture 1.30) pressed against a glass coverslip (NEST, thickness 160–190 μm). The illumination and imaging system includes a 450 nm LED (Daheng Optics, GCI060404) and a camera (Thorlabs, CS165CU/M) to illuminate and image the particle. Two low-pass filters (Andover, 500FL07-25) were used in front of the camera lens to remove the influ-

ence of the backscattered light of the 532 nm laser and photograph clear images of the particle. The Raman-scattered light passed through two 50 : 50 beam splitters (CVI Laser Optics, BTF-VIS-50-2501M-C) and a notch filter (Semrock, NFD01-532-25 × 36) and was focused into the Raman spectrograph. A spectrograph (Zolix, Omni-λ5004i) was used to measure the Stokes-shifted Raman spectrum. A 20 μm entrance slit width and 1200 grooves mm⁻¹ diffraction grating with a blaze wavelength of 500 nm were used to achieve a spectral resolution of 0.021 nm. The wavelength position of the spectrograph was calibrated with an Hg laser. The Raman-scattered light was recorded every 4 s with a range of 624.24–665.40 nm.

As droplets are introduced continuously into the chamber from a medical nebulizer (LANDWIND, PN100), smaller droplets undergo a process of collision and coalescence, leading to the formation of larger droplets that can be readily trapped near the focal point of the laser. In most cases, droplets can be successfully captured within 30 s of the introduction of an aerosol plume into the cell. Air with relative humidity (RH) of 100 % and 0 % was mixed to produce wet air with a desired RH. The flow rates of the humidified and dry airstreams were regulated by mass flow controllers (MFCs; Tianjin Gas Tool Instruments Co., Ltd., Tianjin, China, GT130D), with a combined flow rate of 0.3 L min⁻¹. Two humidity sensors (Sensirion, SHT85) were utilized, with a precision of ±1.5 %. Since the sensor located behind the chamber was positioned in close proximity (~80 mm) to the droplet, its observed values were used as a surrogate for measuring the RH inside the chamber. The RH values were reduced in increments of 5 % every 30 min (Tong et al., 2022; Stewart et al., 2015) until droplet phase separation occurred. The measured values of RH given by the sensors were used as the phase separation RH. Subsequently, the RH level was set to 100 % to investigate the phase mixing of the droplets. The entire experiment was repeated two to four times for each system.

2.3 Determination of phase transitions

When a transparent or weakly absorbing spherical particle is trapped, it can behave as a high-quality factor optical cavity that supports sharp optical resonances, resulting in cavity-enhanced Raman scattering. These resonances can be observed as peaks in the Raman spectrum of a particle and are often referred to as whispering gallery modes (WGMs). In principle, particle morphology can be deduced from the WGMs, as inhomogeneities in the refractive index can disrupt the circulation of the WGMs (Lin et al., 1992; Mitchem et al., 2006). Raman spectra measurements of single droplets in various morphological states are presented in Fig. 1. When the droplet was in a homogeneous phase morphology, the droplet acted as a high-quality microcavity and sharp WGM peaks overlapped with the spontaneous Raman spectrum (Fig. 1a). When the droplet was in a state of a core–

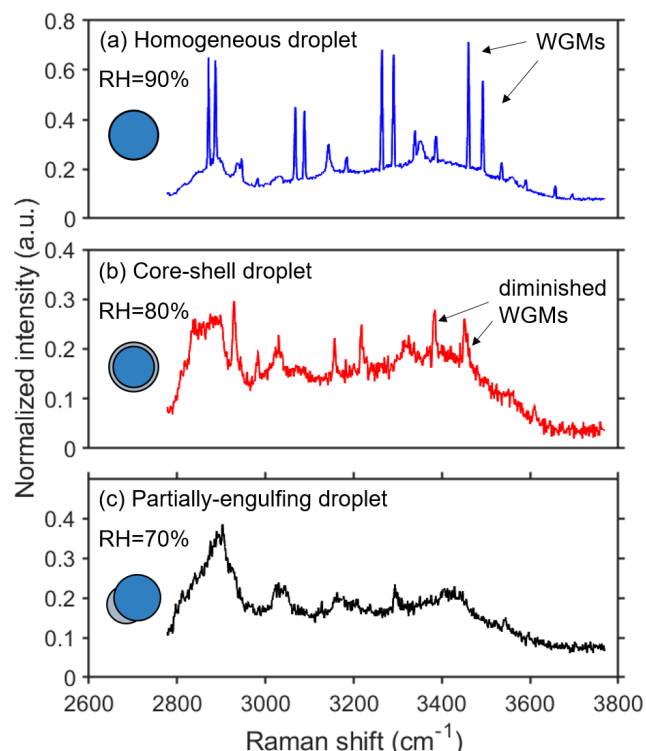


Figure 1. Raman spectra of 3-MGA-II microdroplets: (a) a homogeneous droplet (RH=90%); (b) a core–shell droplet (RH=80%); (c) a partially engulfed droplet (RH=70%). The WGMs are marked by black arrows. The normalization of the peak is achieved by dividing it by the maximum value of the spectrum’s intensity.

shell structure, observed WGMs were clearly diminished in measured spectra (Fig. 1b). The origin of the damping of the WGMs is the radial homogeneity that is present when the particle is separated into a hydrophilic core and a hydrophobic shell. As a result, when fitting the Raman spectra with the Mie-scattering model for homogeneous droplets, the error in the best fits greatly increases. Examination of the retrieved radius and refractive index reveals a clear break with fits for that of a homogeneous sphere. Therefore, the point at which a significant break in the particle size and refractive index occurred can be used as the point at which core–shell phase separation occurs. As illustrated in Fig. 1c, when the droplet was partially engulfed and non-spherical, WGM peaks in the spectrum were absent (Reid et al., 2011). The origins of the spontaneous Raman peaks at 3300 and ~ 3050 cm^{-1} are identified as the spurious or weakened WGM peaks and the vibration of the N–H bond, respectively. Overall, the results of this analysis demonstrate the dynamic changes in the Raman spectra of single droplets as they undergo morphological transitions (Sullivan et al., 2020; Stewart et al., 2015; Tong et al., 2022).

The peak-finding method used in this study is based on the iPeak code developed by O’Haver (2022). In short, the code first smooths the first derivative of the signal and identifies downward-going zero crossings that meet a certain predetermined minimum slope and amplitude threshold. By adjusting the corresponding parameters, it is possible to accurately detect the desired peaks. The algorithm used to fit WGM peaks in spectra from homogeneous spheres in this study was proposed by Preston and Reid (2013, 2015). The algorithm compares observed peak positions to expected positions calculated using a resonance condition from Mie theory. Error is minimized by varying the particle size and refractive index (i.e., the parameters of best fit). The method has been demonstrated to provide a rapid determination of the fitted radius and refractive index with an accuracy of ± 2 nm and ± 0.0005 , respectively. During the experiment with reduced RH, we had to adjust the laser power to ensure the stable capture of droplets, which will affect the peak intensity. To eliminate this effect, as demonstrated by Tong et al. (2022), we normalized all Raman spectra used in this study by the area below the spontaneous Raman signals.

3 Results and discussion

3.1 Phase behaviors of SOA proxy–AS mixed droplets

Figure 2 presents the results of time-resolved Raman spectra of aerosol droplets produced from a 3-MGA-II solution under continuously varying RH, as well as the corresponding particle size and refractive index values. To enable temperature and RH to stabilize, the chamber was conditioned with airflow for 50 min after trapping a particle. During the dehumidification process, the particle diameter decreased from 11.85 to 9.03 μm , and the refractive index increased from 1.379 to 1.475 when RH decreased from 93.0% to 70.0%. The particle size and water content decreased with RH due to the equilibrium partitioning of water molecules between vapor and droplets. Meanwhile, the refractive index of the droplets gradually increased as the water content decreased. When LLPS occurred, the droplets changed from a symmetrical homogeneous phase to either an asymmetrical partially engulfed structure, which led to the disappearance of the WGMs, or a core–shell structure. As RH in the reaction chamber was reduced, the LLPS was initiated, marked by the variations in the WGM signal (see Fig. 1b). This was achieved by reducing RH (setting values) by 5% at 30 min intervals until the organic phase separated from the water-rich phase and then by continuing to decrease RH by 10%–15%. Figure 2a illustrates how the fitting of the droplet diameter and the refractive index deteriorated as the shell developed, indicating phase separation. The refractive index’s shift results from a significant change in the radial profile due to the formation of a core–shell structure. Additionally, the persistence of strong WGMs indicates that the morphology of the droplet remains spherical following LLPS and

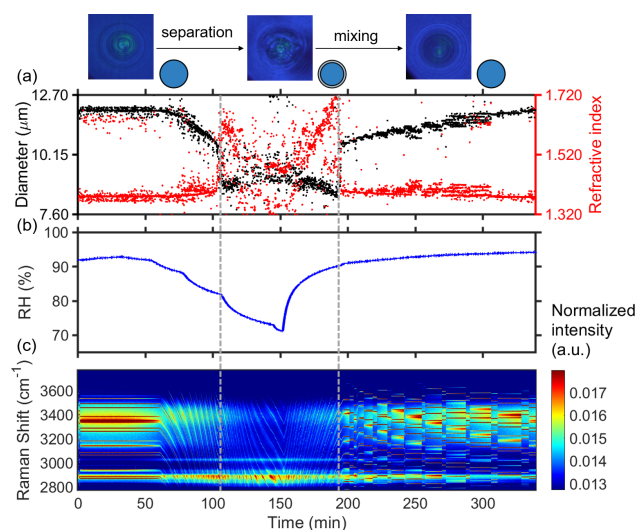


Figure 2. Liquid–liquid phase separation and mixing of aqueous 3-MGA-II. A schematic diagram of phase states is at the top of the figure. (a) Timescale of changes in droplet size and refractive index, determined from fitting the Raman shift positions of the WGMs. (b) RH variation after the trapping chamber during the humidity-changing process. (c) Time-resolved Raman spectra. The cessation of the random motion of inclusions within the droplet and the resultant formation of a core–shell structure are indicated by the dashed grey line on the left. The dashed grey line on the right serves as an indication of the point at which the droplet morphology transitioned from a state of separated phases to a homogeneous phase. The Raman spectra at 53, 113 and 130 min are shown in Fig. 1a, b and c, respectively. Fitting errors of the WGMs are presented in Fig. S3.

is of a core–shell structure. When the RH increased from 70 % to 95 %, the reappearance of the continuously shifting WGM signal was observed, suggesting that the inorganic phase mixed with the organic phase, and the droplet returned to a homogeneous phase. During the humidification process, there is an opposite trend observed in the particle size and refractive index of the droplet compared to the dehumidification process. In conclusion, the variations in the WGM signal can serve as a reliable indicator of the occurrence of liquid–liquid phase separation or mixing, and the RH at these points can be considered the SRH or MRH, respectively. The observed phase transitions of droplets produced from HEXT-IV and HEXD-V solutions are shown in Figs. 3 and 4, respectively.

Figure S2 presents the results of time-resolved Raman spectra of aerosol droplets produced from GL / AS solution under continuously varying RH, as well as the corresponding particle diameter and refractive index values. At the start of the experiment, the chamber RH was held at 93 % for approximately 75 min. The spectrum during this period revealed a clear bright trend, indicative of the presence of many WGMs in the newly captured droplets. As the chamber RH dropped to a minimum value of 71.5 % at around 200 min, the position

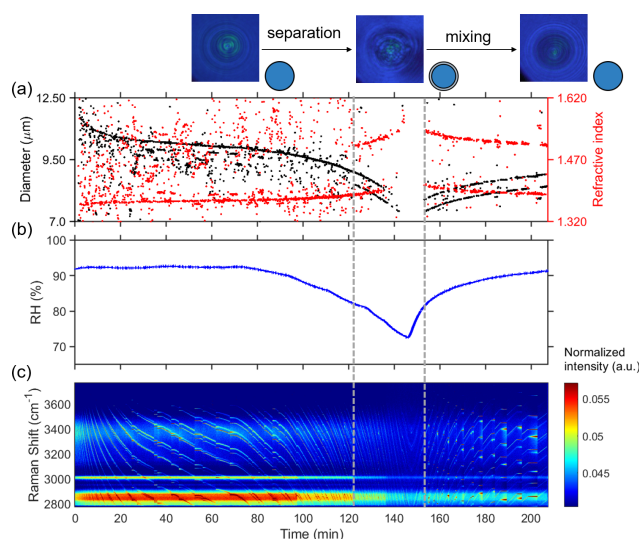


Figure 3. Liquid–liquid phase separation of aqueous HEXT-IV. (a) Timescale of changes in droplet size and refractive index, determined from fitting the Raman shift positions of the WGMs. (b) RH variation after the trapping chamber during the humidity-changing process with time. (c) Time-resolved Raman spectra. The cessation of the random motion of inclusions within the droplet and the resultant formation of a core–shell structure are indicated by the dashed grey line on the left. The dashed grey line on the right serves as an indication of the point at which the droplet morphology transitions from a state of phase separation to a homogeneous phase morphology. This transformation is characterized by the occurrence of phase mixing.

of the WGMs in each spectral snapshot shifted continuously, following the same trend as the chamber RH. This observation suggests that the droplet was homogeneous and that no phase separation occurred in the experimental RH range. The phenomenon regarding the GL / AS system is consistent with the conclusion by Song et al. (2013) and Gorkowski et al. (2020).

3.2 Effect of pH on SRH and MRH of different systems

The SRH and MRH of aerosol droplets produced from 3-MGA-I–3-MGA-VI solution are shown in Fig. 5a and Table S2. The pH of the 3-MGA / AS solution without the addition of an acid or base was 2.70. For solutions with a lower pH (1.19 and 0.48), SA was added, while NaOH was added to solutions with a higher pH (3.70, 5.21 and 6.53) to adjust their pH levels. The SRH values were 92.7 %, 89.5 %, 80.6 %, 79.7 %, 76.2 % and 69.7 % at pH values of 6.53, 5.21, 3.70, 2.70, 1.19 and 0.48, respectively. It is worth mentioning that when the pH of the 3-MGA system is 0.48, only two sets of valid parallel experimental data are available, even though we repeated the experiment several times. Because in other parallel experiments, the SRH of the droplet is lower than the capture range of AOT, the AOT would not

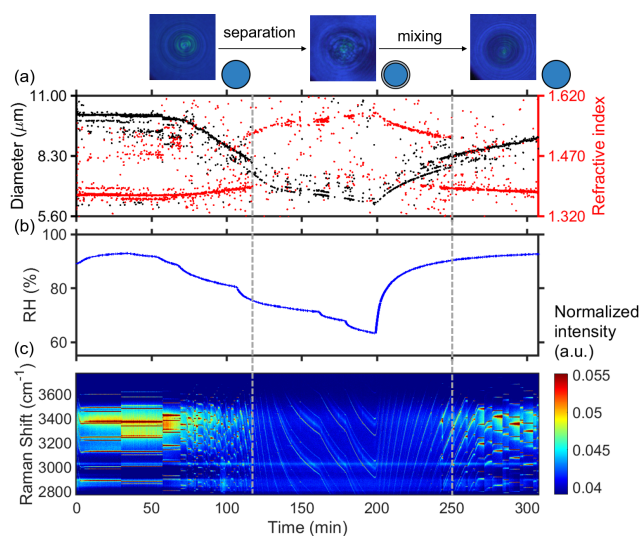


Figure 4. Liquid–liquid phase separation of aqueous HEXD-V. **(a)** Timescale of changes in droplet size and refractive index, determined from fitting the Raman shift positions of the WGMs. **(b)** RH variation after the trapping chamber during the humidity-changing process. **(c)** Time-resolved Raman spectra. The cessation of the random motion of inclusions within the droplet and the resultant formation of a core–shell structure are indicated by the dashed grey line on the left. The dashed grey line on the right serves as an indication of the point at which the droplet morphology transitions from a state of phase separation to a homogeneous phase morphology. This transformation is characterized by the occurrence of phase mixing.

be able to continue the capture when the particle size decreases to $\sim 6 \mu\text{m}$. Therefore, the actual SRH may be a bit lower at this pH, but this does not affect the results we discuss later. With a decrease in pH, ammonium sulfate transforms into ammonium bisulfate. Our results are consistent with the hypothesis that ammonium bisulfate exhibits a weaker salting-out effect compared to ammonium sulfate and thus hinders the ability of organic matter to precipitate out of the solution (Losey et al., 2018). The MRH values at pH values of 6.53, 5.21, 2.70, 1.19 and 0.48 were 87.6 %, 89.5 %, 87.3 %, 83.9 % and 83.5 %, respectively, and are generally higher than corresponding SRH values, especially in the low-pH range (< 5.00). The SRH was higher than the MRH at pH 6.53, which was abnormal because a lower SRH is commonly expected due to the activation barrier. We do not have a specific explanation for this phenomenon, although it should be noted that the observed values were relatively close to each other, indicating that the higher SRH at pH 6.53 might potentially be attributed to experimental error. The hysteresis between SRH and MRH existed because the SRH process has an activation barrier while the MRH process does not, and lower RH is needed for the aerosol droplet to overcome the activation barrier to form two phases (Freedman, 2020). Similar results were also observed in HEXT / AS and HEXD / AS systems. Additionally, the pH-dependent

SRHs obtained in this study were compared to those reported by Losey et al. (2018), as depicted in Fig. 5a. It is worth mentioning that the solute concentration used in our study (50 g L^{-1}) is comparable to Losey et al. (2018) (5.0 wt %), allowing for meaningful comparison of results. Overall, the SRHs of 3-MGA obtained in this study were higher than the results of Losey et al. (2018). When the pH was lower than 3.70, in the 3-MGA system, the present study followed a similar trend to the results of Losey et al. (2018), with the SRH decreasing as the pH decreased. However, when the pH was greater than 3.70, our study showed an opposite trend compared to the results of Losey et al. (2018). The observed discrepancy may be attributed to the distinct ambient conditions of the droplets. The laser levitation results in a spherical morphology, while the optical microscopy involves substrate deposition, leading to a morphology resembling a spherical crown (Tong et al., 2022; Zhou et al., 2014). The underlying reasons for these differences are currently unclear, and further investigations are needed.

In addition to 3-MGA, we also studied two organic / AS systems to investigate how acidity affects the SRH and MRH of aerosols of differing composition. These results are shown in Fig. 5 and tabulated in Table 2. The separation diameter (SD) of 3-MGA / AS ranges from 7.23 to 9.74 μm , with a corresponding separation refractive index (SRI) ranging from 1.362 to 1.515. For HEXT / AS, the SD ranges from 9.01 to 9.90 μm , while the SRI ranges from 1.396 to 1.421. Lastly, the SD of HEXD / AS ranges from 7.45 to 8.97 μm , with the SRI ranging from 1.382 to 1.406. The data suggest that acidity did not have a noticeable effect on the MRH of the various systems. The pH of the HEXT / AS solution without the addition of any acid was 5.11, and SA was utilized to adjust the pH to lower levels (3.14, 2.02 and 0.92). The SRH values of the HEXT / AS system (O : C = 0.50) decreased as the pH decreased, with values of 78.3 %, 76.6 %, 76.4 % and 75.7 % at pH values of 5.11, 3.14, 2.02 and 0.92, respectively. The trend is similar to that of the 3-MGA (O : C = 0.67) system, and the reason why SRH decreased may be due to the acid enhancing the miscibility of organic alcohols and inorganic substances, resulting in a greater difficulty in separating the hydrophobic phase from the water-rich phase (Tong et al., 2022). Still, we observed SRH was not strongly dependent on pH for HEXT / AS compared to the 3-MGA / AS system. This is likely due to the fact that organic alcohols have a large pK_a (e.g., the pK_a of HEXT is 14.3) and therefore exhibit minimal ionization in the pH range studied here (Wade and Simek, 2020). Additionally, the relative molecular interactions between alcohols and water are weaker than those of acids, leading to a weaker dependence of the salting-out ability of AS in the HEXT / AS system. The results of Losey et al. (2018) and Tong et al. (2022) are also depicted in Fig. 5b. Our results differ from those of Losey et al. (2018), who observed a significant decline in SRH as the pH decreased. The specific reason for the discrepancy remains unclear, but we speculate it may be due to different conditions

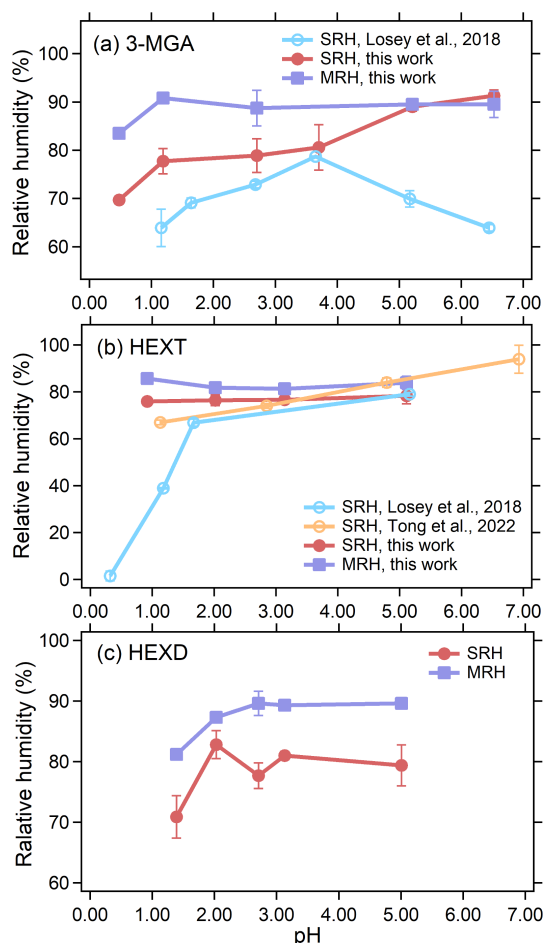


Figure 5. SRHs and MRHs as a function of pH for the (a) 3-MGA / AS system, (b) HEXT / AS system and (c) HEXD / AS system. Unfilled circles represent data from Losey et al. (2018) and Tong et al. (2022). The error bars of SRHs and MRHs are derived from multiple measurements.

of droplets. In contrast to the findings of Tong et al. (2022), our study observed a less pronounced trend in the values of SRH and a narrower range in the distribution of SRH compared to literature values. The difference in OIR between this study (1 : 1) and Tong et al. (2022) (2 : 1) may account for the discrepancy in SRH. Previous studies (Ma et al., 2021; Stewart et al., 2015; Song et al., 2012) indicated that OIR differences could affect SRH, but SRH was not significantly dependent on OIR. The discrepancy in SRH may also be due to the variations in experimental conditions, such as laser power or experimental duration. For the HEXD / AS ($O : C = 0.33$) system, the pH of the the HEXD / AS solution without the addition of any acid was 5.01, and SA was used to adjust the pH to lower levels (3.13, 2.71, 2.03 and 1.39). SRH decreased significantly when the pH was less than 2.00, while acidity had no significant effect on SRH when the pH was greater than 2.00, with values of 79.4 %, 81.0 %, 77.7 %, 82.8 % and 70.9 % at pH values of 5.01, 3.13, 2.71, 2.03

and 1.39, respectively. This phenomenon was attributed to a mechanism similar to that observed in HEXT / AS. To our knowledge, this is the first investigation on the pH-dependent phase transition of HEXD / AS at the single-particle level in a contact-free environment.

The pH values of misty cloud and fog droplets typically fall within the range of 2 to 7, whereas continental and marine aerosol particles display a broader spectrum of pH values (Pye et al., 2020; Tilgner et al., 2021). Our research suggests that in real atmospheric conditions, phase separation behavior of droplets may be influenced significantly by their acidity. It is challenging to measure the droplet pH of the investigated system using AOT. However, previous studies (Coddens et al., 2019; Li et al., 2023) have shown that at high RH (90 %–100 %), the difference in the pH values between droplets and bulk solution is relatively small. Therefore, we used bulk solution pH as an indicator of pH at the droplet phase transition. This study focused on volatile organics and was conducted over a relatively long period, which may have affected our results. Nevertheless, the organic compounds used in this study have low volatility. For instance, the vapor pressure of 3-MGA is 7.41×10^{-7} to 2.92×10^{-4} mmHg (DTXSID50871000, United States Environmental Protection Agency), compared to normal volatile organic components of atmospheric aerosol such as 2-methyl-1-propanol with a vapor pressure of 10.5 to 16.4 mmHg (DTXSID0021759, United States Environmental Protection Agency). Volatility information about other organics is provided in Table S5. Also, the influence of droplet size change in our system can be neglected. For example, as shown in Fig. 2, the droplet size was basically the same at the beginning and the end of the experiment at the same RH of 93.0 % (11.85 μm at the beginning and 11.79 μm at the end).

3.3 Effect of O : C on phase separation behavior in different systems

Our findings provide evidence that phase separation of droplets persists even when the organic–inorganic system is adjusted to a specific level of acidity. An important determinant of whether droplets undergo phase separation is the O : C ratio. To illustrate this, we have included a plot in Fig. S4, which showcases the experimental system used in our study alongside relevant literature values. One point that needs to be declared is Fig. S4 is only plotted for systems with no additional H_2SO_4 or NaOH. As shown in Fig. S4, our findings, as well as those from previous studies (You et al., 2013; O’Brien et al., 2015), indicated that there is no correlation between the occurrence of LLPS and the hydrogen-to-carbon (H : C) ratios of the organics, which is consistent with results in previous findings (Bertram et al., 2011; Song et al., 2012). However, a clear trend was observed between LLPS occurrence and the O : C ratio of the organic components. We observed that droplets of 3-MGA / AS, HEXT / AS and HEXD / AS systems with O : C between

Table 2. SRH information for each pH studied as well as the initial diameter, separation diameter (SD), separation refractive index (SRI), MRH, mixing diameter (MD) and mixing refractive index (MRI) data.

3-MGA / AS system (O : C = 0.67)							
Initial pH	Initial diameter (μm)	SRH (%)	SD (μm)	SRI ($\lambda = 650 \text{ nm}$)	MRH (%)	MD (μm)	MRI ($\lambda = 650 \text{ nm}$)
0.48	10.97 \pm 1.57	69.7 \pm 0.2	7.23 \pm 1.72	1.515 \pm 0.086	83.5	6.82	1.540
1.19	11.23 \pm 1.20	77.7 \pm 2.6	8.68 \pm 2.38	1.454 \pm 0.100	90.8 \pm 0.2	9.08 \pm 1.64	1.394 \pm 0.009
2.70	12.02 \pm 2.94	78.9 \pm 3.5	7.88 \pm 1.21	1.493 \pm 0.082	88.7 \pm 3.7	6.81 \pm 2.76	1.506 \pm 0.094
3.70	10.87 \pm 1.87	80.6 \pm 4.7	7.24 \pm 1.00	1.491 \pm 0.088			
5.21	11.06 \pm 1.63	89.0 \pm 0.9	8.93 \pm 0.16	1.362 \pm 0.014	89.5	7.89	1.381
6.53	13.73 \pm 0.41	91.3 \pm 1.2	9.74 \pm 0.36	1.444 \pm 0.187	89.5 \pm 2.7	7.89 \pm 0.06	1.383 \pm 0.01
HEXT / AS system (O : C = 0.50)							
0.92	13.52 \pm 1.6	75.9 \pm 0.2	9.90 \pm 0.76	1.421 \pm 0.017	85.7	10.83	1.420
2.02	12.88 \pm 1.0	76.4 \pm 2.3	9.09 \pm 0.46	1.409 \pm 0.007	81.8	9.34	1.410
3.14	12.31 \pm 0.8	76.6 \pm 1.5	9.01 \pm 0.47	1.408 \pm 0.002	81.3	9.04	1.409
5.11	13.53 \pm 0.4	78.3 \pm 3.4	9.15 \pm 0.35	1.396 \pm 0.014	83.9 \pm 2.8	9.04 \pm 0.73	1.412
HEXD / AS system (O : C = 0.33)							
1.39	11.48 \pm 0.78	70.9 \pm 3.5	7.45 \pm 0.77	1.406 \pm 0.008	81.2	7.93	1.406
2.03	10.54 \pm 0.57	82.8 \pm 2.3	7.90 \pm 0.99	1.382 \pm 0.007	87.3	8.83	1.392
2.71	14.55 \pm 1.36	77.7 \pm 2.1	8.30 \pm 0.28	1.391 \pm 0.009	89.6 \pm 2.0	8.53 \pm 0.32	1.388 \pm 0.010
3.13	11.02 \pm 0.62	81.0 \pm 0.7	8.97 \pm 0.22	1.384 \pm 0.016	89.3	9.14	1.384
5.01	12.22 \pm 2.73	79.4 \pm 3.4	8.33 \pm 0.40	1.384 \pm 0.019	89.6 \pm 0.1	8.38 \pm 0.54	1.390 \pm 0.004

0.33 and 0.67 undergo LLPS. With the decrease in water content in the droplets, two distinct phases were formed: an organic-rich phase and a salt-rich aqueous phase, under both acidic and neutral conditions. By contrast, no LLPS occurred in the GL / AS system, as shown in Fig. S2. In general, particles with low O : C are more prone to undergoing LLPS. This observation is consistent with the findings of Song et al. (2012), who reported that LLPS was never observed when O : C > 0.80 and always observed when O : C < 0.56.

As shown in Fig. 2 and Table S2, for most spectra, WGMs remained after LLPS occurred for droplets of 3-MGA / AS. This phenomenon indicates that the droplets undergo LLPS with a core–shell morphology in most conditions, which is consistent with the prediction of Gorkowski et al. (2020). Meanwhile, the morphology of phase-separated droplets containing either HEXT or HEXD was also mostly core–shell-shaped, as depicted in Figs. 3 and 4 and Tables S3 and S4. This is attributed to the lower interfacial tension observed at higher O : C, leading to a higher possibility of conditions for forming core–shell-shaped droplets (Gorkowski et al., 2020). These findings support the idea that the O : C ratio plays a crucial role in determining the morphology of phase-separated particles in organic–inorganic mixed aerosols.

4 Conclusions

The aim of this study is to investigate the effect of pH and O : C on the phase transition behavior of levitated particles

using AOT. Our results show that across aerosol pH in atmospheric conditions, the presence of sulfuric acid inhibited the LLPS of aerosol droplets that contained organics (3-MGA, HEXT, HEXD) and AS. Additionally, the MRHs were found to be higher than the SRHs. The O : C ratio of phase-separating systems is 0.67, 0.50 and 0.33, and by contrast, LLPS of the high-O : C system (GL, O : C = 1.00) did not occur. Meanwhile, the morphology of levitated aerosol particles was studied, and we found that 42 out of 46 droplets that underwent LLPS formed a core–shell structure. The SRH of all experimental systems ranged from $\sim 70\%$ to 90% . In certain cases, as the RH decreased, the droplet morphology changed from core–shell to partially engulfed, which is similar to the findings reported by Kucinski et al. (2020). However, as the RH further decreased, the droplet particle size became smaller than $6\mu\text{m}$, making it impossible to capture the droplets using AOT. Consequently, in most instances, we were unable to observe the droplet morphology at RH levels below 70% . The results presented here provide new insights into the behavior of different types of aerosol droplets, and the findings have important implications for our understanding of physical and chemical processes that occur in the atmosphere. It is anticipated that future studies will be carried out to examine the OIR-dependent phase separation in real acidified ambient aerosols. Such research will provide insights into the morphological characteristics of real aerosols and the ways in which these characteristics influence important properties such as hygroscopicity and homo-

geneous chemistry. Such information will be helpful in furthering our understanding of the impacts of ambient aerosols on the environment and human health.

Additionally, in situ pH measurement or pH estimation methods, such as the real-time AOT analysis in microdroplets reported by Boyer et al. (2020), could be combined with SRH measurements for a more accurate and comprehensive analysis. Furthermore, our study used a surrogate for SOA instead of in situ measurements of real SOA, which can be addressed in future work by using SOA generated from a smog chamber or real SOA precursors and oxidized species.

Data availability. The data used in this paper can be obtained from the corresponding author upon request.

Supplement. The supplement related to this article is available online at: <https://doi.org/10.5194/acp-23-10255-2023-supplement>.

Author contributions. YC built the instrument, performed the experiments, analyzed the data, plotted the figures and wrote the original draft. XP conceptualized the study; contributed to instrumentation, data analysis and discussion; and reviewed the manuscript. HL and CX contributed to the instrumentation and discussion. YM contributed to the experiments and discussion. ZX and FZ contributed to the discussion and manuscript review. TCP contributed to data analysis and manuscript review. ZW administrated the project, conceptualized the study, reviewed the manuscript and contributed to funding acquisition.

Competing interests. At least one of the (co-)authors is a member of the editorial board of *Atmospheric Chemistry and Physics*. The peer-review process was guided by an independent editor, and the authors also have no other competing interests to declare.

Disclaimer. Publisher's note: Copernicus Publications remains neutral with regard to jurisdictional claims in published maps and institutional affiliations.

Financial support. This research has been supported by the National Natural Science Foundation of China (grant nos. 91844301, 42005087 and 42005086), Key Research and Development Program of Zhejiang Province (grant nos. 2021C03165 and 2022C03084), and the Fundamental Research Funds for the Central Universities (grant no. 2018QNA6008).

Review statement. This paper was edited by Guangjie Zheng and reviewed by two anonymous referees.

References

- Angle, K. J., Crocker, D. R., Simpson, R. M. C., Mayer, K. J., Garofalo, L. A., Moore, A. N., Mora Garcia, S. L., Or, V. W., Srinivasan, S., Farhan, M., Sauer, J. S., Lee, C., Pothier, M. A., Farmer, D. K., Martz, T. R., Bertram, T. H., Cappa, C. D., Prather, K. A., and Grassian, V. H.: Acidity across the interface from the ocean surface to sea spray aerosol, *P. Natl. Acad. Sci. USA*, 118, e2018397118, <https://doi.org/10.1073/pnas.2018397118>, 2021.
- Bertram, A. K., Martin, S. T., Hanna, S. J., Smith, M. L., Bodsworth, A., Chen, Q., Kuwata, M., Liu, A., You, Y., and Zorn, S. R.: Predicting the relative humidities of liquid-liquid phase separation, efflorescence, and deliquescence of mixed particles of ammonium sulfate, organic material, and water using the organic-to-sulfate mass ratio of the particle and the oxygen-to-carbon elemental ratio of the organic component, *Atmos. Chem. Phys.*, 11, 10995–11006, <https://doi.org/10.5194/acp-11-10995-2011>, 2011.
- Boyer, H. C., Gorkowski, K., and Sullivan, R. C.: In situ pH measurements of individual levitated microdroplets using aerosol optical tweezers, *Anal. Chem.*, 92, 1089–1096, <https://doi.org/10.1021/acs.analchem.9b04152>, 2020.
- Canagaratna, M. R., Jimenez, J. L., Kroll, J. H., Chen, Q., Kessler, S. H., Massoli, P., Hildebrandt Ruiz, L., Fortner, E., Williams, L. R., Wilson, K. R., Surratt, J. D., Donahue, N. M., Jayne, J. T., and Worsnop, D. R.: Elemental ratio measurements of organic compounds using aerosol mass spectrometry: characterization, improved calibration, and implications, *Atmos. Chem. Phys.*, 15, 253–272, <https://doi.org/10.5194/acp-15-253-2015>, 2015.
- Ciobanu, V. G., Marcolli, C., Krieger, U. K., Weers, U., and Peter, T.: Liquid-Liquid Phase Separation in Mixed Organic/Inorganic Aerosol Particles, *J. Phys. Chem. A*, 113, 10966–10978, 2009.
- Coddens, E. M., Angle, K. J., and Grassian, V. H.: Titration of aerosol pH through droplet coalescence, *J. Phys. Chem. Lett.*, 10, 4476–4483, <https://doi.org/10.1021/acs.jpcclett.9b00757>, 2019.
- Corral Arroyo, P., David, G., Alpert, P. A., Parmentier, E. A., Ammann, M., and Signorell, R.: Amplification of light within aerosol particles accelerates in-particle photochemistry, *Science*, 376, 293–296, <https://doi.org/10.1126/science.abm7915>, 2022.
- Cosman, L. M., Knopf, D. A., and Bertram, A. K.: N₂O₅ reactive uptake on aqueous sulfuric acid solutions coated with branched and straight-chain insoluble organic surfactants, *J. Phys. Chem. A*, 112, 2386, <https://doi.org/10.1021/jp710685r>, 2008.
- Cui, X., Tang, M., Wang, M., and Zhu, T.: Water as a probe for pH measurement in individual particles using micro-Raman spectroscopy, *Anal. Chim. Acta.*, 1186, 339089, <https://doi.org/10.1016/j.aca.2021.339089>, 2021.
- Fang, T., Guo, H., Zeng, L., Verma, V., Nenes, A., and Weber, R. J.: Highly acidic ambient particles, soluble metals, and oxidative potential: a link between sulfate and aerosol toxicity, *Environ. Sci. Technol.*, 51, 2611–2620, <https://doi.org/10.1021/acs.est.6b06151>, 2017.
- Freedman, M. A.: Phase separation in organic aerosol, *Chem. Soc. Rev.*, 46, 7694–7705, <https://doi.org/10.1039/C6CS00783J>, 2017.
- Freedman, M. A.: Liquid-liquid phase separation in supermicrometer and submicrometer aerosol particles, *Acc. Chem. Res.*, 53, 1102–1110, <https://doi.org/10.1021/acs.accounts.0c00093>, 2020.

- Freedman, M. A., Hasenkopf, C. A., Beaver, M. R., and Tolbert, M. A.: Optical properties of internally mixed aerosol particles composed of dicarboxylic acids and ammonium sulfate, *J. Phys. Chem. A*, 113, 13584–13592, <https://doi.org/10.1021/jp906240y>, 2009.
- Gong, Z. Y., Pan, Y. L., Videen, G., and Wang, C. J.: Optical trapping and manipulation of single particles in air: principles, technical details, and applications, *J. Quant. Spectrosc. Ra.*, 214, 94–119, <https://doi.org/10.1016/j.jqsrt.2018.04.027>, 2018.
- Gorkowski, K., Donahue, N. M., and Sullivan, R. C.: Emulsified and liquid-liquid phase-separated states of alpha-pinene secondary organic aerosol determined using aerosol optical tweezers, *Environ. Sci. Technol.*, 51, 12154–12163, <https://doi.org/10.1021/acs.est.7b03250>, 2017.
- Gorkowski, K., Donahue, N. M., and Sullivan, R. C.: Aerosol optical tweezers constrain the morphology evolution of liquid-liquid phase-separated atmospheric particles, *Chem*, 6, 204–220, <https://doi.org/10.1016/j.chempr.2019.10.018>, 2020.
- Guo, H., Liu, J., Froyd, K. D., Roberts, J. M., Veres, P. R., Hayes, P. L., Jimenez, J. L., Nenes, A., and Weber, R. J.: Fine particle pH and gas–particle phase partitioning of inorganic species in Pasadena, California, during the 2010 CalNex campaign, *Atmos. Chem. Phys.*, 17, 5703–5719, <https://doi.org/10.5194/acp-17-5703-2017>, 2017.
- Kucinski, T. M., Dawson, J. N., and Freedman, M. A.: Size-Dependent Liquid-Liquid Phase Separation in Atmospherically Relevant Complex Systems, *J. Phys. Chem. Lett.*, 10, 6915–6920, <https://doi.org/10.1021/acs.jpcllett.9b02532>, 2019.
- Kucinski, T. M., Ott, E.-J. E., and Freedman, M. A.: Flash Freeze Flow Tube to Vitrify Aerosol Particles at Fixed Relative Humidity Values, *Anal. Chem.*, 92, 5207–5213, <https://doi.org/10.1021/acs.analchem.9b05757>, 2020.
- Kucinski, T. M., Ott, E. E., and Freedman, M. A.: Dynamics of liquid-liquid phase separation in submicrometer aerosol, *J. Phys. Chem. A*, 125, 4446–4453, <https://doi.org/10.1021/acs.jpca.1c01985>, 2021.
- Lam, H. K., Xu, R., Choczynski, J., Davies, J. F., Ham, D., Song, M., Zuend, A., Li, W., Tse, Y.-L. S., and Chan, M. N.: Effects of liquid–liquid phase separation and relative humidity on the heterogeneous OH oxidation of inorganic–organic aerosols: insights from methylglutaric acid and ammonium sulfate particles, *Atmos. Chem. Phys.*, 21, 2053–2066, <https://doi.org/10.5194/acp-21-2053-2021>, 2021.
- Li, M., Kan, Y., Su, H., Pöschl, U., Parekh, S. H., Bonn, M., and Cheng, Y. F.: Spatial homogeneity of pH in aerosol microdroplets, *Chem*, 9, 1036–1046, <https://doi.org/10.1016/j.chempr.2023.02.019>, 2023.
- Lin, H. B., Eversole, J. D., and Campillo, A. J.: Continuous-wave stimulated Raman scattering in microdroplets, *P. Opt. Lett.*, 17, 828–830, <https://doi.org/10.1364/ol.17.000828>, 1992.
- Losey, D. J., Parker, R. G., and Freedman, M. A.: pH Dependence of Liquid–Liquid Phase Separation in Organic Aerosol, *J. Phys. Chem. Lett.*, 7, 3861–3865, <https://doi.org/10.1021/acs.jpcllett.6b01621>, 2016.
- Losey, D. J., Ott, E. J. E., and Freedman, M. A.: Effects of high acidity on phase transitions of an organic aerosol, *J. Phys. Chem. A*, 122, 3819–3828, <https://doi.org/10.1021/acs.jpca.8b00399>, 2018.
- Ma, S., Chen, Z., Pang, S., and Zhang, Y.: Observations on hygroscopic growth and phase transitions of mixed 1, 2, 6-hexanetriol/(NH₄)₂SO₄ particles: investigation of the liquid–liquid phase separation (LLPS) dynamic process and mechanism and secondary LLPS during the dehumidification, *Atmos. Chem. Phys.*, 21, 9705–9717, <https://doi.org/10.5194/acp-21-9705-2021>, 2021.
- Mahrt, F., Newman, E., Huang, Y., Ammann, M., and Bertram, A. K.: Phase behavior of hydrocarbon-like primary organic aerosol and secondary organic aerosol proxies based on their elemental oxygen-to-carbon ratio, *Environ. Sci. Technol.*, 55, 12202–12214, <https://doi.org/10.1021/acs.est.1c02697>, 2021.
- Mikhailov, E. F., Pöhlker, M. L., Reinmuth-Selzle, K., Vlasenko, S. S., Krüger, O. O., Fröhlich-Nowoisky, J., Pöhlker, C., Ivanova, O. A., Kiselev, A. A., Krempel, L. A., and Pöschl, U.: Water uptake of subpollen aerosol particles: hygroscopic growth, cloud condensation nuclei activation, and liquid–liquid phase separation, *Atmos. Chem. Phys.*, 21, 6999–7022, <https://doi.org/10.5194/acp-21-6999-2021>, 2021.
- Mitchem, L., Buajareern, J., Ward, A. D., and Reid, J. P.: A strategy for characterizing the mixing state of immiscible aerosol components and the formation of multiphase aerosol particles through coagulation, *J. Phys. Chem. B*, 110, 13700–13703, <https://doi.org/10.1021/jp062874z>, 2006.
- O'Brien, R. E., Wang, B. B., Kelly, S. T., Lundt, N., You, Y., Bertram, A. K., Leone, S. R., Laskin, A., and Gilles, M. K.: Liquid-liquid phase separation in aerosol particles: imaging at the nanometer scale, *Environ. Sci. Technol.*, 49, 4995–5002, <https://doi.org/10.1021/acs.est.5b00062>, 2015.
- O'Haver, T. C.: A pragmatic introduction to signal processing with applications in scientific measurement, Kindle Direct Publishing, ISBN 9798611266687, 2022.
- Ohno, P. E., Qin, Y., Ye, J., Wang, J., Bertram, A. K., and Martin, S. T.: Fluorescence aerosol flow tube spectroscopy to detect liquid–liquid phase separation, *ACS Earth Space Chem.*, 5, 1223–1232, <https://doi.org/10.1021/acsearthspacechem.1c00061>, 2021.
- Ott, E.-J. E., Tackman, E. C., and Freedman, M. A.: Effects of Sucrose on Phase Transitions of Organic/Inorganic Aerosols, *ACS Earth Space Chem.*, 4, 591–601, <https://doi.org/10.1021/acsearthspacechem.0c00006>, 2020.
- Petters, M. D. and Kreidenweis, S. M.: A single parameter representation of hygroscopic growth and cloud condensation nucleus activity, *Atmos. Chem. Phys.*, 7, 1961–1971, <https://doi.org/10.5194/acp-7-1961-2007>, 2007.
- Preston, T. C. and Reid, J. P.: Accurate and efficient determination of the radius, refractive index, and dispersion of weakly absorbing spherical particle using whispering gallery modes, *J. Opt. Soc. Am. B*, 30, 2113–2122, <https://doi.org/10.1364/JOSAB.30.002113>, 2013.
- Preston, T. C. and Reid, J. P.: Determining the size and refractive index of microspheres using the mode assignments from Mie resonances, *J. Opt. Soc. Am. A*, 32, 2210–2217, <https://doi.org/10.1364/JOSAA.32.002210>, 2015.
- Pye, H. O. T., Nenes, A., Alexander, B., Ault, A. P., Barth, M. C., Clegg, S. L., Collett Jr., J. L., Fahey, K. M., Hennigan, C. J., Herrmann, H., Kanakidou, M., Kelly, J. T., Ku, I.-T., McNeill, V. F., Riemer, N., Schaefer, T., Shi, G., Tilgner, A., Walker, J. T., Wang, T., Weber, R., Xing, J., Zaveri, R. A., and Zuend, A.: The acid-

- ity of atmospheric particles and clouds, *Atmos. Chem. Phys.*, 20, 4809–4888, <https://doi.org/10.5194/acp-20-4809-2020>, 2020.
- Rafferty, A., Vennes, B., Bain, A., and Preston, T. C.: Optical trapping and light scattering in atmospheric aerosol science, *Phys. Chem. Chem. Phys.*, 25, 7066–7089, <https://doi.org/10.1039/d2cp05301b>, 2023.
- Redding, B., Schwab, M. J., and Pan, Y. L.: Raman spectroscopy of optically trapped single biological micro-particles, *Sensors*, 15, 19021–19046, <https://doi.org/10.3390/s150819021>, 2015.
- Reid, J. P., Dennis-Smith, B. J., Kwamena, N. O. A., Miles, R. E. H., Hanford, K. L., and Homer, C. J.: The morphology of aerosol particles consisting of hydrophobic and hydrophilic phases: hydrocarbons, alcohols and fatty acids as the hydrophobic component, *Phys. Chem. Chem. Phys.*, 13, 15559–15572, <https://doi.org/10.1039/c1cp21510h>, 2011.
- Rosenfeld, D., Sherwood, S., Wood, R., and Donner, L.: Climate effects of aerosol-cloud interactions, *Science*, 343, 379–380, <https://doi.org/10.1126/science.1247490>, 2014.
- Song, M., Marcolli, C., Krieger, U. K., Zuend, A., and Peter, T.: Liquid-liquid phase separation in aerosol particles: dependence on O:C, organic functionalities, and compositional complexity, *Geophys. Res. Lett.*, 39, L19801, <https://doi.org/10.1029/2012GL052807>, 2012.
- Song, M. J., Marcolli, C., Krieger, U. K., Lienhard, D. M., and Peter, T.: Morphologies of mixed organic/inorganic/aqueous aerosol droplets, *Faraday Discuss.*, 165, 289–316, <https://doi.org/10.1039/c3fd00049d>, 2013.
- Stewart, D. J., Cai, C., Nayler, J., Preston, T. C., Reid, J. P., Krieger, U. K., Marcolli, C., and Zhang, Y. H.: Liquid-liquid phase separation in mixed organic/inorganic single aqueous aerosol droplets, *J. Phys. Chem. A*, 119, 4177–4190, <https://doi.org/10.1021/acs.jpca.5b01658>, 2015.
- Sullivan, R. C., Boyer-Chelmo, H., Gorkowski, K., and Beydoun, H.: Aerosol Optical Tweezers Elucidate the Chemistry, Acidity, Phase Separations, and Morphology of Atmospheric Microdroplets, *Acc. Chem. Res.*, 11, 2498–2509, <https://doi.org/10.1021/acs.accounts.0c00407>, 2020.
- Tilgner, A., Schaefer, T., Alexander, B., Barth, M., Collett Jr., J. L., Fahey, K. M., Nenes, A., Pye, H. O. T., Herrmann, H., and McNeill, V. F.: Acidity and the multiphase chemistry of atmospheric aqueous particles and clouds, *Atmos. Chem. Phys.*, 21, 13483–13536, <https://doi.org/10.5194/acp-21-13483-2021>, 2021.
- Tong, Y. K., Meng, X. X. Y., Zhou, B., Sun, R., Wu, Z. J., Hu, M., and Ye, A. P.: Detecting the pH-dependent liquid-liquid phase separation of single levitated aerosol microdroplets via laser tweezers-Raman spectroscopy, *Front. Phys.*, 10, 969921, <https://doi.org/10.3389/fphy.2022.969921>, 2022.
- Wade, L. G. and Simek, J. W.: Acidity of alcohols and phenols, in: *Organic Chemistry*, <https://chem.libretexts.org/@go/page/45234> (last access: 4 April 2023), 2020.
- Wang, M., Zheng, N., Zhao, D., Shang, J., and Zhu, T.: Using micro-Raman spectroscopy to investigate chemical composition, mixing states, and heterogeneous reactions of individual atmospheric particles, *Environ. Sci. Technol.*, 55, 10243–10254, <https://doi.org/10.1021/acs.est.1c01242>, 2021.
- Weber, R. J., Guo, H. Y., Russell, A. G., and Nenes, A.: High aerosol acidity despite declining atmospheric sulfate concentrations over the past 15 years, *Nat. Geosci.*, 9, 282–285, <https://doi.org/10.1038/ngeo2665>, 2016.
- You, Y., Renbaum-Wolff, L., and Bertram, A. K.: Liquid-liquid phase separation in particles containing organics mixed with ammonium sulfate, ammonium bisulfate, ammonium nitrate or sodium chloride, *Atmos. Chem. Phys.*, 13, 11723–11734, <https://doi.org/10.5194/acp-13-11723-2013>, 2013.
- You, Y., Smith, M. L., Song, M., Martin, S. T., and Bertram, A. K.: Liquid-liquid phase separation in atmospherically relevant particles consisting of organic species and inorganic salts, *Int. Rev. Phys. Chem.*, 33, 43–77, <https://doi.org/10.1080/0144235X.2014.890786>, 2014.
- Young, A. H., Keene, W. C., Pszenny, A. A. P., Sander, R., Thornton, J. A., Riedel, T. P., and Maben, J. R.: Phase partitioning of soluble trace gases with size-resolved aerosols in near-surface continental air over northern Colorado, USA, during winter, *J. Geophys. Res.-Atmos.*, 118, 9414–9427, <https://doi.org/10.1002/jgrd.50655>, 2013.
- Zheng, G., Su, H., Wang, S., Andreae, M., Pöschl, U., and Cheng, Y.: Multiphase buffer theory explains contrasts in atmospheric aerosol acidity, *Science*, 369, 1374–1377, <https://doi.org/10.1126/science.aba3719>, 2020.
- Zhou, Q., Pang, S.-F., Wang, Y., Ma, J.-B., and Zhang, Y.-H.: Confocal Raman studies of the evolution of the physical state of mixed phthalic acid/ammonium sulfate aerosol droplets and the effect of substrates, *J. Phys. Chem. B*, 118, 6198–6205, <https://doi.org/10.1021/jp5004598>, 2014.